Chemical Papers (2020) 74:3717–3725
https://doi.org/10.1007/s11696-020-01251-w

ORIGINAL PAPER

Tetra- and hexanuclear copper(I) iminothiolate complexes: synthesis, structures, and solid-state thermochromic dual emission in visible and near-infrared regions

Yoshiki Ozawa[1] · Marino Mori[1] · Hidetoshi Kiyooka[1] · Yuumi Sugata[1] · Toshikazu Ono[2] · Masaaki Abe[1]

Received: 13 February 2020 / Accepted: 13 June 2020 / Published online: 22 June 2020

Abstract

Two new photoluminescent multinuclear Cu(I) cluster complexes supported by monoanionic bidentate ligand *N*-methylbenzimidazolethiolate (Me-bimt$^-$), [Cu_n(Me-bimt)$_n$] with $n=4$ (**1**) and 6 (**2**), have been synthesized and structurally characterized by single-crystal X-ray diffraction analysis. For **1** and **2**, the Cu(I) ions and the Me-bimt$^-$ ligands construct a cubane-type {Cu_4S_4} and a hexagonal-prism {Cu_6S_6} frameworks, respectively. In the crystalline state, complexes **1** and **2** exhibit green ($\lambda_{em}=500$ nm) and near-infrared ($\lambda_{em}=876$ nm) emission, respectively, under UV irradiation ($\lambda_{ex}=365$ nm) at room temperature. Both crystals reveal temperature-dependent dual emission below 200 K: complex **1** emits in the visible wavelength region ($\lambda_{em}=493$ and 542 nm) and complex **2** in the visible to near-infrared wavelength region ($\lambda_{em}=752$ and 973 nm) which are attributed to multiple photoexcited states at the cluster frameworks with distinct metal nuclearity.

Keywords Copper(I) · Cluster compounds · Crystal structure · Thermochromic dual emission · Near-infrared emission

Introduction

Multinuclear transition-metal complexes with d^{10} electronic configuration, such as copper(I) and silver(I), show rich photoluminescent behavior associated with multiple photo-excited states such as metal-to-ligand charge transfer (MLCT), multi-metal cluster-centered (CC) charge transfer, and inter-ligand (IL) transition (Yam and Lo 1999). In some cases, radiative decay from two distinct photoexcited states simultaneously occurs, which represents the "dual emission" phenomenon (Ford et al. 1999).

Monoanionic iminothiolato (N=C–S$^-$) bidentate ligands such as pyridinethiolate and imidazolethiolate are able to link two or more metal centers to form multinuclear cluster complexes (Ford and Vogler 1993). Many literature studies are available for crystal structures of the iminothiolato multicopper(I) complexes with a tetrameric {Cu_4S_4} core and a hexameric, hexagonal pillar-type {Cu_6S_6} core, but only a few studies have been reported so far on their photophysical properties (Kundu et al. 2014; Xie et al. 2005). Such multicopper(I) complexes are typically formed via spontaneous self-assembly of the corresponding metallic sources and ligands mixed together with the appropriate molar ratio in solution, but the synthetic methodology to precisely control the metal nuclearity (e.g., the number of metal centers in a single molecule) of products remains yet, in general, to be established for transition-metal coordination complexes. Herein we describe the synthesis, molecular structures, and solid-state photoluminescence properties of two new Cu(I) iminothiolate clusters formulated [Cu_n(Me-bimt)$_n$] with $n=4$ (**1**)

This work was presented at the International Conference on Coordination and Bioinorganic Chemistry held in Smolenice during June 2–7, 2019.

This paper is dedicated to Professor Milan Melník for his outstanding contribution to coordination and bioinorganic chemistry.

Electronic supplementary material The online version of this article (https://doi.org/10.1007/s11696-020-01251-w) contains supplementary material, which is available to authorized users.

✉ Yoshiki Ozawa
ozawa@sci.u-hyogo.ac.jp

✉ Masaaki Abe
mabe@sci.u-hyogo.ac.jp

[1] Graduate School of Material Science, University of Hyogo, 3-2-1 Kouto, Kamigori-Cho, Ako-Gun, Hyogo 789-1297, Japan

[2] Graduate School of Engineering, Kyushu University, 744 Moto-oka, Nishi-Ku, Fukuoka 819-0395, Japan

and 6 (**2**), where Me-bimt$^-$ is a monoanionic bidentate ligand *N*-methylbenzimidazolethiolate(1–). The synthetic conditions employed gave initially a crude solid containing both tetramer **1** and hexamer **2** but the individual clusters were subsequently transformed to either form by adopting appropriate solvent combinations for recrystallization. Selective isolation of **1** and **2** has been unambiguously confirmed by single-crystal X-ray diffraction analyses. We show that both compounds exhibit temperature-dependent dual emission in the solid state upon UV excitation, wherein **1** exhibits thermochromic dual emission in the visible region and **2** from visible to near-infrared (NIR) region.

Experimental

Materials and methods

Chemical reagents and solvents used in this study were purchased from TCI and WAKO and used without further purification unless otherwise stated. All of the synthetic reactions in this study were performed under Ar atmosphere.

Apparatus and equipment

IR measurements were performed on a JASCO FT/IR-4000 at 298 K by an attenuated total reflectance (ATR) method. ^{1}H NMR spectroscopy was performed at 600 MHz on a JEOL ECA-600 and a JEOL ECZ-600R/S1 spectrometers using $CDCl_3$ as solvents, and TMS was employed as an internal standard to determine the chemical shift. Elemental analysis was carried out by the Laboratory for Organic Elemental Microanalysis, Kyoto University. UV–Vis diffuse reflectance spectra (DRS) were measured by a JASCO V-670 UV–Vis–NIR spectrometer with an ISN-723 integrating sphere attachment. Luminescence spectra of the single crystals were measured by a Hamamatsu PMA-11 (C7473-46) spectrometer (190–900 nm) and an Ocean Optics FLAME-S spectrometer (600–1100 nm). The crystalline samples were placed in a Linkam THMS600 temperature-controlled (78–293 K) microscope stage. A Panasonic UJ-20 UV-LED system was used as an excitation light source (λ_{ex} = 365 nm). The emission from the solid samples was introduced to the optical fibers of the spectrometer through a microscope. Lifetimes and quantum yields of solid-state photoluminescence were measured on a Hamamatsu Quantaurus-Tau C11367-02 fluorescence lifetime spectrometer and Quantaurus-QY C11347 absolute PL yield spectrometer, respectively.

Synthesis and characterization

Synthesis of (triphenylmethyl)sulfanylbenzimidazole (Tr-bimt).

This compound was prepared according to the literature procedure (Doerge and Cooray 1991). A solution of benzimidazole-2-thiol (bimtH) (4.2 g, 28 mmol), trityl chloride (8.0 g, 28 mmol), and Et_3N (3.1 g, 28.5 mmol) in dry THF (150 mL) was stirred for 8 h at 293 K. The resulting suspension was filtered to remove triethylammonium salt which was washed thoroughly with THF. The combined filtrate was concentrated by evaporation to dryness under reduced pressure. The white solid of Tr-bimt was identified by ^{1}H NMR spectroscopy as a mono-THF adduct. Yield: 10.1 g (92%). The obtained product was used in the following synthesis without further purification. ^{1}H NMR (600 MHz, $CDCl_3$, 298 K) δ 7.70 (d, 1H, J = 8.22 Hz, benzimidazole 7-H), 7.64 (s, 1H, N*H*), 7.47 (d, 6H, J = 6.9 Hz, trityl group *ortho* H), 7.33–7.27 (m, 9H, trityl group *meta* and *para* H), 7.19–7.12 (m, 2H, benzimidazole 5,6-H), 6.99 (d, 1H, J = 7.6 Hz, benzimidazole 4-H), 3.75 (t, 4H, THF –O–CH_2–CH_2–), 1.85 (m, 4H, THF –O–CH_2–CH_2–).

Synthesis of methyl-2-(triphenylmethyl) sulfanylbenzimidazole (Tr–Me-bimt).

This compound was obtained by a modified method of the literature (Doerge and Cooray 1991). Ground powder of KOH (7.0 g, 125 mmol) was placed in a round-bottom flask (500 mL) and dried under vacuum for 3 h. To this was added a solution of Tr-bimt–THF adduct (10.0 g, 25.5 mmol) in dry acetone (170 mL) followed by MeI (5.9 g, 41 mmol), and the mixture was stirred for 1 h at 293 K. The resulting pale-yellow solution was filtered to remove a suspended solid of KOH. The filtrate was added to toluene (700 mL), and the mixture was divided into two portions which were washed first with water (150 mL) and second with a saturated aqueous solution of NaCl (150 mL). After combining the individual solutions, the solution was dried over anhydrous Na_2SO_4 and was concentrated by evaporation to dryness under reduced pressure. Yield: 7.1 g (68%). The yellow solid of Tr–Me-bimt as a crude product was used in the following synthesis without further purification. ^{1}H NMR (600 MHz, $CDCl_3$, 298 K) δ 7.31–7.27 (m, 15H, trityl group), 7.23–7.12 (m, 4H, benzimidazole 4,7-H), 3.75 (s, 3H, CH_3).

Synthesis of *N*-methyl-benzimidazolethiol (Me-bimtH).

A solution of Tr–Me-bimt (7.1 g, 16.9 mmol) in acetic acid (7.5 mL)–MeOH (142.5 mL) was heated under contentious

stirring for 5 h at 358 K. The resulting yellow solution was concentrated by evaporation to dryness under reduced pressure. The yellow solid was dissolved in CH_2Cl_2 (150 mL) and was washed with an aqueous solution of 10% sodium bicarbonate (100 mL × 3). The organic layer was dried over anhydrous Na_2SO_4 and concentrated by evaporation to dryness under reduced pressure. The light-yellow crude product was collected by filtration and washed with toluene to remove unreacted Tr–Me-bimt. The obtained white powder was identified by ^{1}H NMR spectroscopy. Yield: 1.59 g (58%). ^{1}H NMR ($CDCl_3$, 600 MHz, 298 K) δ 10.68 (s, br, 1H, SH), 7.27–7.20 (m, 1H, benzimidazole 7-H), 7.23 (ddd, 2H, J = 6.9, 6.5, and 1.4 Hz, benzimidazole 5,6-H), 7.17–7.15 (m, 1H, benzimidazole 4-position), 3.79 (s, 3H, CH_3).

Synthesis of *N*-methyl-benzimidazolethiolatocopper(I) [Cu_n(Me-bimt)$_n$] (n = 4 and 6).

A solution of Me-bimtH (0.092 g, 0.6 mmol) with Et_3N (0.151 g, 1.5 mmol) in CH_3CN (10 mL) was added dropwise to a solution of $[Cu(CH_3CN)_4]CF_3SO_3$ (0.196 g, 0.5 mmol) in CH_3CN (10 mL) under continuous stirring at 293 K. The resulting pale-yellow suspension was heated under continuous stirring for 2 h at 323 K. A white solid formed was separated by filtration, washed with CH_3CN, and dried under vacuum. This preparative procedure gave a mixture of two species [Cu_n(Me-bimt)$_n$] with n = 4 and 6 on the basis of elemental analysis and ^{1}H NMR spectroscopy. Yield: 0.102 g (87%). Anal. Calcd. for $C_8H_7CuN_2S$: C, 42.37; H, 3.11; N, 12.35%. Found: C, 42.45; H, 3.01; N, 12.18%.

Separated recrystallization and single-crystal X-ray structure analysis for [Cu_4(Me-bimt)$_4$] (1) and [Cu_6(Me-bimt)$_6$] (2).

Single crystals of **1** were grown at 293 K as colorless block-shaped crystals from a toluene solution of the above-mentioned mixture by layering and slowly diffusing Et_2O. Single crystals of **2** were obtained at 303 K as red platelet-shaped crystals from a CH_2Cl_2 solution of the mixture by layering and slowly diffusing CH_3CN. Single-crystal X-ray diffraction measurements were performed at 290 and 150 K for both crystals on a Rigaku Rapid image plate diffractometer using Mo $K\alpha$ (λ = 0.7107 Å) radiation. The crystal was attached to a thin Nylon loop and kept under a cold N_2 gas stream from a He gas-expansion cryostat. All non-hydrogen atoms were refined anisotropically, and hydrogen atoms were placed at the calculated positions and treated according to the riding model during refinements. All the calculations for structure determination and refinements were carried out using WinGX (Farrugia 2012) crystallographic software suite with SHELXL-2016/6 refinement program (Sheldrick 2015). For the refinement of **1**, the structure was treated as a two-component twin using TWIN and BASF commands in the SHELXL program. It was found that the final R value for **1** was lower at high temperature (290 K, R = 0.091) than low temperature (150 K, R = 0.119), allowing us the high-temperature data to use for structural discussion. In contrast, free from the twin problem, the results for structural analysis of **2** were satisfactory at both temperatures (150 K, R = 0.052; 290 K, R = 0.064). Under these circumstances, the 290-K data were employed for both complexes for their structural description and comparison.

Crystallographic data of **1** (T = 290 K): $C_{32}H_{28}Cu_4N_8S_4$, M_r = 907.02, colorless prism, 0.34 × 0.34 × 0.28 mm^3, monoclinic, space group $C2/c$ (No. 15), a = 20.307(2), b = 15.107(1), c = 15.185(1) Å, β = 132.511(2)°, V = 3434.0(4) Å^3, $\mu(\lambda = 0.7107$ Å) = 2.73 mm^{-1}, Z = 4, θ_{max} = 30.0°, 20,220 reflections measured, 4976 unique (R_{int} = 0.07) which were used in all calculations. The final R = 0.091, $wR(F^2)$ = 0.318, and GOF = 1.09 (all data).

Crystallographic data of **2** (T = 290 K): $C_{48}H_{42}Cu_6N_{12}S_6$, M_r = 1360.53, red platelet, 0.20 × 0.15 × 0.07 mm^3, trigonal, space group R-3 (No. 142), a = 13.479(2), c = 24.061(3) Å, V = 3786.0(10) Å^3, $\mu(\lambda = 0.7107$ Å) = 2.78 mm^{-1}, Z = 3, θ_{max} = 30.0°, 15,063 reflections measured, 2445 unique (R_{int} = 0.073 which were used in all calculations. The final R = 0.064, $wR(F^2)$ = 0.233 and GOF = 1.17(all data).

CCDC reference numbers for **1** are 1,981,286 (290 K) and 1,981,287 (150 K) and those for **2** are 1,981,293 (290 K) and 1,981,294 (150 K).

Density functional theory (DFT) calculations

DFT calculations were carried out with the ADF2019 suite of programs (Baerends et al. 2019; te Velde et al. 2001). The geometrical parameters for **1** and **2** were taken from the crystal structures. Geometry optimizations were performed with applying S_4 and D_{3d} molecular symmetry to **1** and **2**, respectively. Exchange correlation function (XC) of PW91 method was applied for calculations. The valence shell atomic orbitals of Cu, S, N, C, and H atoms were described by triple-zeta Slater-type basis sets with two polarization functions (ADF database TZ2P).

Results and discussion

Synthesis and crystallization

We have synthesized and isolated single crystals of tetranuclear complex [Cu_4(Me-bimt)$_4$] (**1**) and hexanuclear complex [Cu_6(Me-bimt)$_6$] (**2**), as shown in Fig. 1. The reaction of $[Cu(CH_3CN)_4]CF_3SO_3$ with a slight excess of Me-bimtH in CH_3CN in the presence of Et_3N (2 h, 323 K) gave an

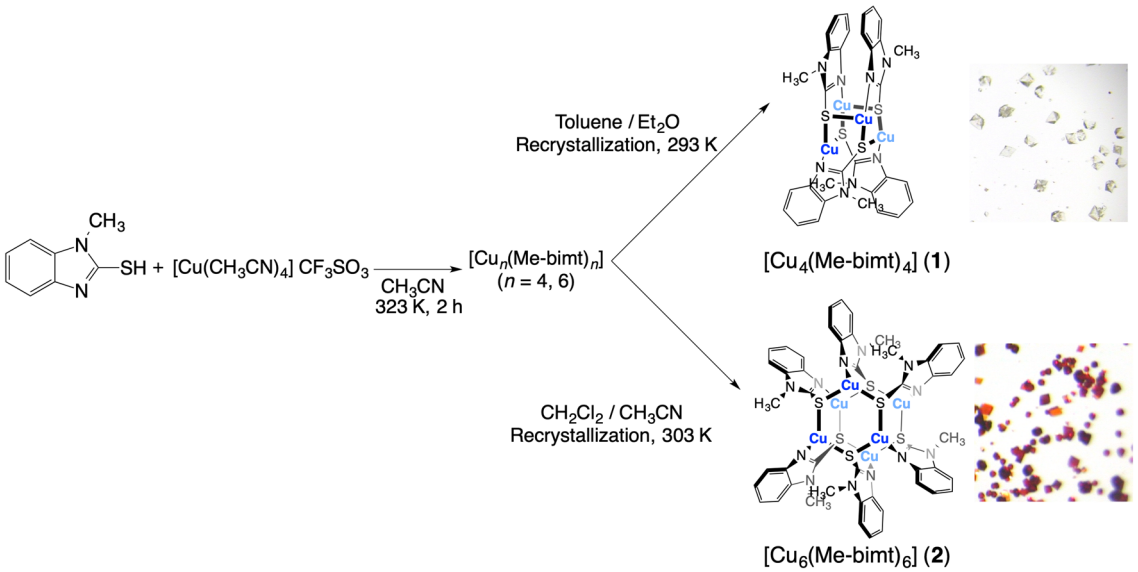

Fig. 1 Schematic of preparation and crystallization procedures of **1** and **2**. Photographic images of the crystalline solid are also shown

off-white solid which was identified as mixture of two species $[Cu_n(Me\text{-}bimt)_n]$ with $n = 4$ and 6 (87% yield). Selective isolation of either form was successfully achieved by recrystallization of the mixture by the use of appropriate solvent combination. Thus, complexes **1** and **2** were crystallized separately at room temperature from toluene/Et_2O and CH_2Cl_2/CH_3CN systems, respectively. Interestingly, the color of the crystals is markedly different, e.g., colorless and deep red for **1** and **2**, respectively. It is noted that when lower temperature conditions (such as 273 K) were applied complex **2** was contaminated with **1**, implying an equilibrium between **1** and **2** in solution. The formation of the off-white solid during the synthetic reaction may infer that complex **1** is a kinetic product.

We have also found a reversible transformation between **1** and **2** upon recrystallization by appropriate solvent choice mentioned above. Thus, recrystallization of red crystals **2** from toluene/Et_2O gave colorless crystals **1** to be deposited from the solution. Similarly, recrystallization of colorless crystals **1** from CH_2Cl_2/CH_3CN results in the deposition of red crystals **2**. The solvent combination thus leads to a complete control over metal nuclearity of products as a crystal. There are only a few previous reports for such a separation of tetrameric and hexameric Cu(I) complexes in preparative procedures (Chivers et al. 2001; Yue et al. 2009). In the current study, we have shown not only a complete separation but also a reversible conversion between tetramer and hexamer through recrystallization.

A qualitative insight has been gained for solution equilibrium between **1** and **2** by ^{1}H NMR spectroscopy. Dissolution of either crystal, **1** or **2**, in $CDCl_3$ at room temperature was found to give, within minutes, a light-yellow clear solution. Figure 2 shows ^{1}H NMR spectrum of a $CDCl_3$ solution prepared by dissolution of **1** at 295 K, wherein two groups of resonances were observed for the benzimidazole moiety with labels (*a*–*e*) for the larger intensity group (defined as group **A**) and (*a'*–*e'*) for the smaller (defined as group **B**). Here, either group is tentatively assigned to **1** or **2**. The chemical shift data ($CDCl_3$, 600 MHz, 295 K) and the assignment are as follows. Group **A**: δ 7.32, 7.04, 6.93, 6.63 (s, 1H × 4, aromatic protons of the benzimidazole moiety), and 3.46 (s, 3H, CH_3). Group **B**: δ 7.35, 6.96, 6.80, 6.38 (s, 1H × 4, aromatic protons of the benzimidazole moiety), and 3.23 (s, 3H, CH_3). The observed **B/A** ratio in intensity was 0.4. Slightly broadened resonances may infer the presence of exchange between two species on the NMR timescale. Further study, including variable-temperature NMR spectroscopy, is necessary to describe in more detail the dynamics and kinetics of these clusters in solution.

Single-crystal X-ray diffraction study

The molecular structures of **1** and **2** were unambiguously determined by single-crystal X-ray diffraction analysis. The molecular structure and the $\{Cu_4S_4\}$ framework of **1** at 290 K are depicted in Fig. 3. Selected interatomic distances and bond angles are listed in Table 1. Complex **1** crystallizes in the monoclinic space group *C*2/*c* and has a cuboidal $\{Cu_4S_4\}$ framework, wherein four Cu(I) centers are bridged by N and S atoms from the bidentate Me-bimt$^-$ ligands (Fig. 3a). In the crystalline lattice, a twofold rotation axis parallel to the *b*-axis penetrates the molecule and half of the molecule is crystallographically independent. The whole molecule has virtually an S_4 symmetry.

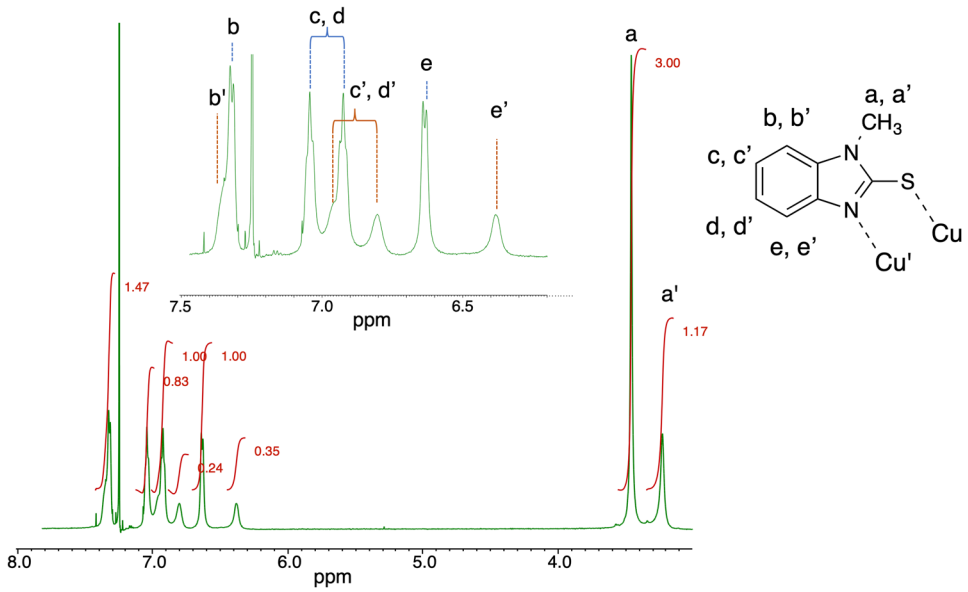

Fig. 2 A ^{1}H NMR spectrum (600 MHz, 295 K) of a $CDCl_3$ solution prepared upon dissolution of crystals of **1**. Note that two different species labeled as (a–e) and (a'–e') were readily formed in the room-temperature solution; these are described in the main text as groups **A** and **B**, respectively. Inset: the proton labeling scheme for the benzimidazolate moiety

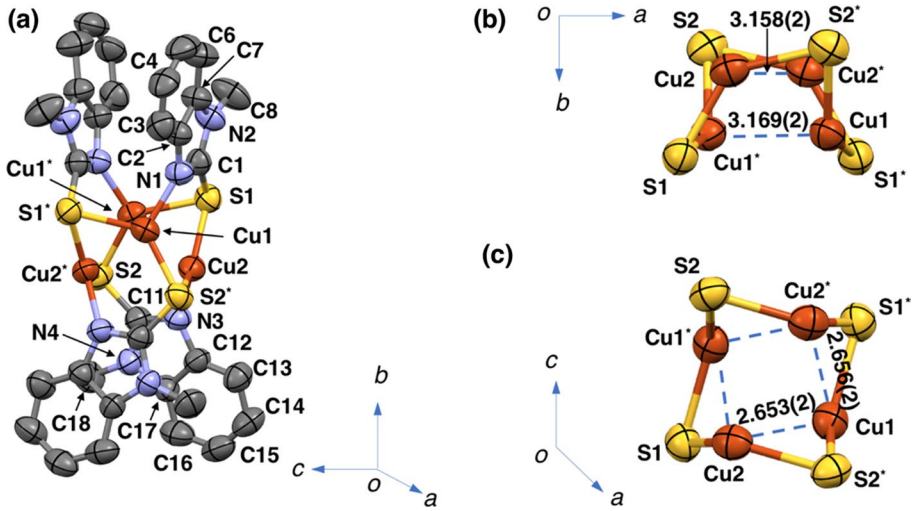

Fig. 3 ORTEP diagrams of **1** at 290 K with thermal ellipsoids at a 50% probability level. Hydrogen atoms are omitted for clarity. **a** The molecular structure. **b** The $\{Cu_4S_4\}$ framework projected along the *c*-axis and **c** that along the *b*-axis. For **b** and **c**, Cu•••Cu distances (Å) are given. Symmetry code: (*) –*x*, *y*, 1/2–*z*

Table 1 Selected interatomic distances (Å) and bond angles (°) of **1** at 290 K

Interatomic distances			
Cu1•••Cu2	2.653(2)	Cu1•••Cu2*	2.656(2)
Cu1•••Cu1*	3.169(2)	Cu2•••Cu2*	3.158(2)
Cu1—S1*	2.339(3)	Cu2—S2*	2.349(3)
Cu1—S2*	2.234(3)	Cu2—S1	2.235(3)
Cu1—N1	1.989(7)	Cu2—N3	1.993(6)
Bond angles			
S2*—Cu1—S1*	130.95(9)	S1—Cu2—S2*	130.65(9)
N1—Cu1—S2*	122.4(2)	N3—Cu2—S1	122.2(2)
N1—Cu1—S1*	106.4(2)	N3—Cu2—S2*	106.8(2)
Cu2—S1—Cu1*	70.95(8)	Cu1*—S2—Cu2*	70.71(8)

Symmetry code: (*) –*x*, *y*, 1/2–*z*

The Cu(I) centers adopt a highly distorted, three-coordinate geometry with an "NS_2" donor set. Four Cu(I) and four S atoms provided from Me-bimt$^-$ form a cuboidal $\{Cu_4S_4\}$ framework (Fig. 3b) with a tub-shaped, eight-membered $\{Cu_4S_4\}$ ring (Fig. 3c). Interatomic separations between two Cu(I) centers perpendicular to the molecular S_4 axis (Cu1•••Cu1* and Cu2•••Cu2*) are 3.158(2) and 3.169(2) Å (Fig. 3b). In contrast, four other Cu•••Cu contacts (Cu1•••Cu2, Cu1•••Cu2*, Cu1*•••Cu2, and Cu1*•••Cu2*) are much shorter, 2.653(2) and 2.656(2) Å (Fig. 3c) and these are also shorter than the summation of van der Waals radii (2.8 Å). The observed Cu•••Cu separations and tetragonal compression (along the *b*-axis) of the $\{Cu_4\}$ core in **1** are typical of those found in

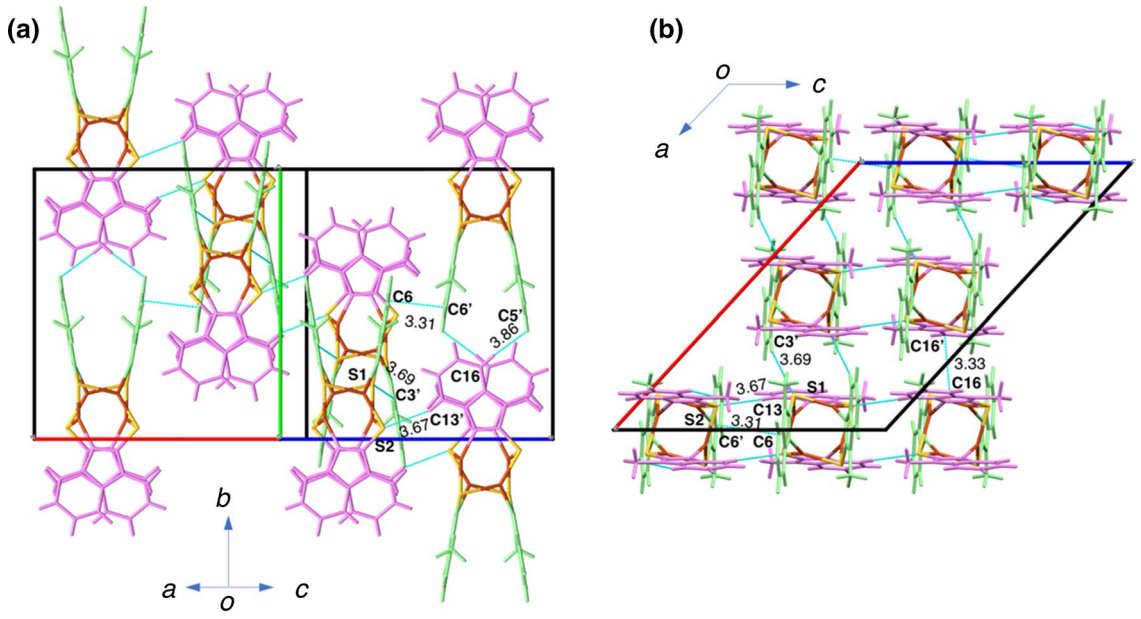

Fig. 4 Stick-model representations for crystal packing of **1** at 290 K. **a** Projected along the *a**-axis (on the *bc* plane). **b** Projected along the *b*-axis. Two sets of symmetry-equivalent ligand moieties are drawn as pink and light-green sticks. Interatomic contacts within the sum of the van der Waals radii are indicated as broken cyan lines

imidazolethiolate tetracopper(I) complexes reported earlier (Raper et al. 1991; Venkatesh et al. 2014).

Crystal packing of **1** is illustrated in Fig. 4. Selected intermolecular contacts are listed in Table S1 (Supplementary data). The molecules are aligned along the *b*-axis to form 1D columns via intermolecular van der Waals contacts between benzene ring moieties in Mebimt⁻ (C16•••C5′, 3.86(2) Å) (Fig. 4a). In addition, weak *π*–*π* contacts (C6•••C6′, 3.31(3); C16•••C16, 3.33(2) Å) and C–H•••S contacts (S1•••C3′, 3.69(1); C13•••S2′, 3.67(2) Å) are observed among molecules in the *ac*-plane (Fig. 4b).

The molecular structure and $\{Cu_6S_6\}$ framework of **2** at 290 K are depicted in Fig. 5. Selected interatomic distances and bond angles are listed in Table 2. Complex **2** crystallizes in the trigonal space group *R*-3. Two hexagonal $\{Cu_3S_3\}$ moieties are located mutually in an *anti*-parallel fashion to form the $\{Cu_6S_6\}$ framework, and six planar Mebimt⁻ ligands support the distorted $\{Cu_6\}$ octahedron to form a six-bladed paddle-like shape (Fig. 5a). The whole

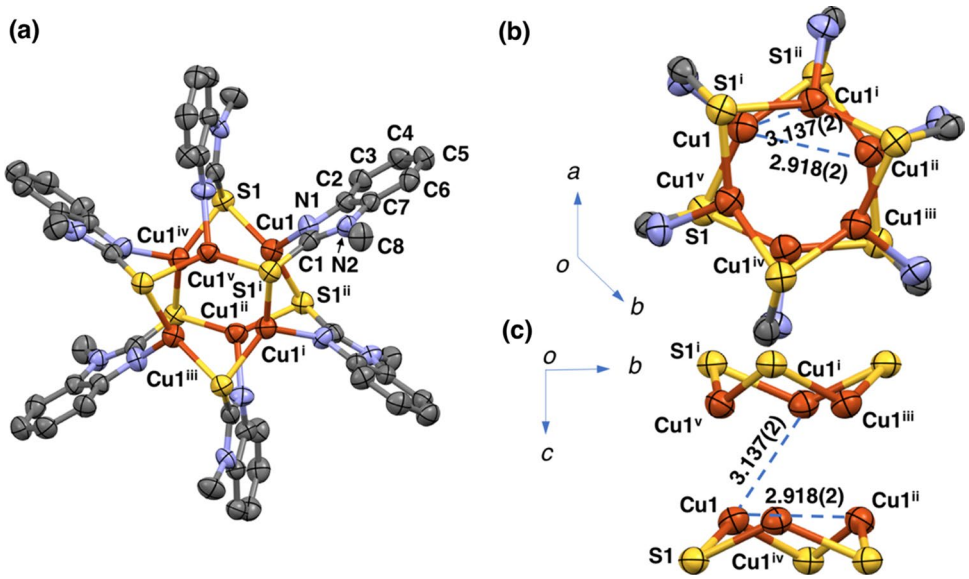

Fig. 5 ORTEP diagrams of **2** at 290 K with thermal ellipsoids at a 50% probability level. Hydrogen atoms are omitted for clarity. **a** The molecular structure. **b** The $\{Cu_6S_6\}$ framework along the *c*-axis and **c** that along the *a*-axis. For **b** and **c**, Cu···Cu distances (Å) are given. Symmetry codes: (i) 2/3 + *x*–*y*, 1/3 + *x*, 4/3–*z*; (ii) 1–*y*, 1+*x*–*y*, *z*; (iii) 2/3–*x*, 4/3–*y*, 4/3–*z*; (iv) –*x* + *y*, 1–*x*, *z*; (v) 1/3 + *y*, 1/3–*x* + *y*, 4/3–*z*

Table 2 Selected interatomic distances (Å) and bond angles (°) of **2** at 290 K

Interatomic distances			
Cu1•••Cu1^{i}	3.137(2)	Cu1—S1	2.266(2)
Cu1•••Cu1^{ii}	2.918(2)	Cu1—S1^{ii}	2.259(2)
		Cu1—N1^{i}	2.004(2)
Bond angles			
S1^{ii}—Cu1—S1	124.85(10)	N1^{i}—Cu1—S1	111.7(2)
Cu1^{iv}—S1—Cu1	80.31(8)	N1^{i}—Cu1—S1^{ii}	116.3(2)

Symmetry codes: (i) 2/3 + *x*–*y*, 1/3 + *x*, 4/3–*z*; (ii) 1–*y*, 1 + *x*–*y*, *z*; (iv) –*x* + *y*, 1–*x*, *z*

molecule has a threefold rotoinversion axis with an exact S_6 symmetry, in which one Cu(I) and one Me-bimt$^-$ are crystallographically independent. The Cu•••Cu distances are 3.137(2) and 2.918(2) Å (Fig. 5b), indicating trigonal elongation of the {Cu_6} core (Fig. 5c). Each Cu(I) adopts three-coordinate geometry with an "N_2S" donor set.

Crystal packing of **2** is shown in Fig. 6. Selected interatomic contacts are listed in Table S2 (Supplementary data). The molecules are engaged each other like "gears" with π•••π contacts between neighboring ligands (C6•••C7′, 3.40(1) Å) to form a 2D layer (Fig. 6a) which is perpendicular to the *c*-axis (Fig. 6b).

Diffuse reflectance spectra (DRS) and density functional theory (DFT) calculations

UV–Vis DRS of colorless crystals of **1** display a single band centered at 335 nm and is transparent in the visible region, as shown in Fig. S1 (Supplementary data). In contrast, deep red crystals of **2** exhibit a low-energy, weaker shoulder at 460 nm in addition to a high-energy, stronger band at 330 nm as shown in Fig. S2 (Supplementary data), the former of which causes the coloration of **2**.

To gain insights into absorption properties of **1** and **2**, especially to identify the nature of visible coloration in **2**, DFT calculations have been carried out. The results are shown in Figs. S3 and S4 (Supplementary data). Irrespective of the metal nuclearity, the highest occupied molecular orbital (HOMO) is assigned to an admixture of (Cu 3d, S 3p) orbitals in the {Cu_nS_n} cores (n = 4 or 6) which are nonbonding in character. In contrast, the nature of the lowest unoccupied molecular orbital (LUMO) is different between the two complexes. The LUMO for **1** is localized to the benzimidazole moiety (ligand-π^* orbital) (Fig. S3) whereas that of **2** is ascribed to an admixture of (Cu 4 s/4p, S 4 s/4p) orbitals in the {Cu_6S_6} core which is bonding in character (Fig. S4). The LUMO level in **2** becomes lower than the ligand-π^* orbital (second LUMO) in energy. The decrease in the LUMO level of **2** relative to **1** is ascribable to electronic delocalization over the {Cu_6S_6} core (Ford et al. 1999; Sabin et al. 1992; Yue et al. 2009). The high-energy bands in DRS for both complexes (330 and 335 nm for **1** and **2**, respectively) are attributed to "{C_nS_n} cluster-to-ligand" charge-transfer transitions. The low-energy band for **2**, corresponding to the narrower HOMO–LUMO gap, is attributable to "{C_6S_6} cluster-centered" transitions in the {Cu_6S_6} core.

Solid-state photoluminescence

In the crystalline state, both compounds are emissive under UV illumination (λ_{ex} = 365 nm). The photoluminescence

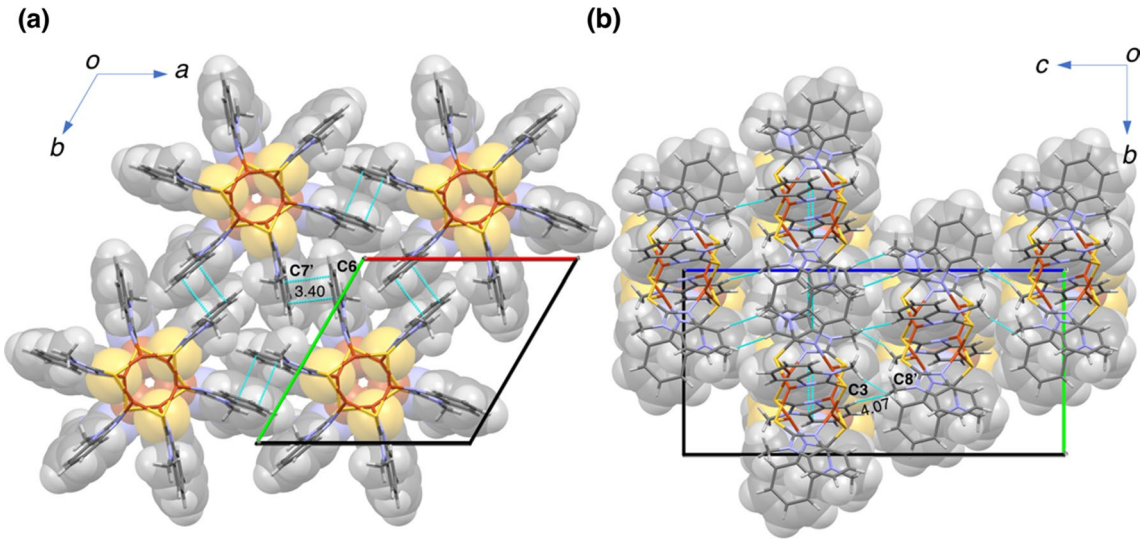

Fig. 6 Stick- and space-fill model representations of the crystal packing of **2** at 290 K. **a** Projected along the *c*-axis. **b** Projected along the *a*-axis. Intermolecular contacts within the sum of the van der Waals radii are indicated as broken cyan lines

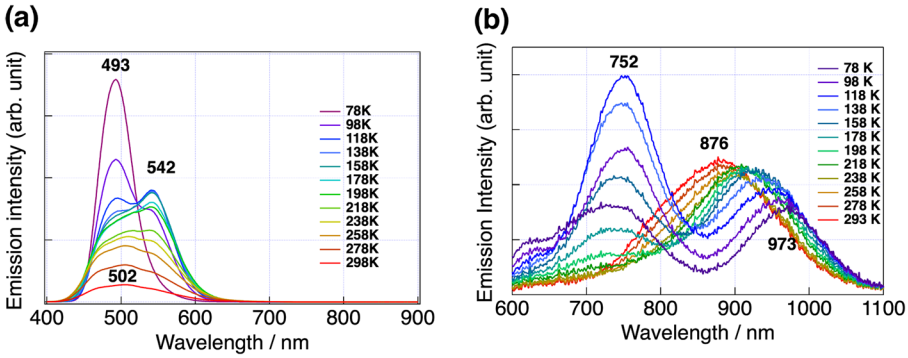

Fig. 7 Temperature-dependent solid-state photoluminescence spectra (λ_{ex} = 365 nm) of **a** **1** (T = 78 to 298 K) and **b** **2** (T = 78 to 293 K)

spectra of **1** and **2** at various temperatures are shown in Fig. 7, which reveals a markedly contrast in luminescence depending on the metal nuclearity and temperature.

At 293 K, complex **1** emits in greenish-blue with a broad emission band centered at 502 nm (Fig. 7a). The emission quantum yield was $\Phi = 0.16$ at 293 K. The emission lifetime of $\tau = 11$ µs at 293 K suggests phosphorescence from a triplet state. Intensity of this emission increased as the temperature was decreased. Below 200 K, dual-emissive character became apparent with the higher energy (HE) peak at 493 nm and the lower energy (LE) peak at 542 nm. Further decrease in temperature led to the decrease in the LE intensity with concomitant growth of the HE band. At 78 K, single emission, derived from the HE band, is observed with a complete lack of the LE band. In the dual-emissive temperature region, the energy of LE and HE bands remains less affected but the intensity of both is highly temperature dependent. On the basis of the emission lifetime and the DFT analysis for **1** described above, we tentatively assign the LE (λ_{em} = 542 nm) and HE emissions (λ_{em} = 493 nm) to "{Cu_4S_4} cluster-to-ligand" charge-transfer and "{Cu_4S_4} cluster-centered" excited states, respectively. We note that the thermochromic dual-emissive character for iminothiolate tetracopper(I) clusters is reported herein for the first time, though it has been of extensive interest for cubane-type [$Cu_4I_4L_4$] clusters (Benito et al. 2015; De Angelis et al. 2006; Ford et al. 1999; Huitorel et al. 2018; Kitagawa et al. 2010; Nagaoka et al. 2018; Perruchas et al. 2010; Yang et al. 2016).

The thermochromic dual luminescence is also observed for **2** but occurs in the NIR region (Fig. 7b). The emission intensity of **2** is much weaker than that of **1**. The temperature-dependent spectral change for **2** appears more complex than that in **1**. At 293 K, complex **2** gives a single, broad emission band centered at 876 nm. Similar to **1**, the emission lifetime of **2** is of microsecond order, $\tau = 1.7$ µs at 293 K, indicating phosphorescence from a triplet state. The emission quantum yield is $\Phi = 0.01$ at 293 K. Upon cooling, the emission band shifts to a lower energy side with maintaining the single emission feature. At 218 K, an additional HE emission band begins to grow at ca. 720 nm. Further cooling leads to dual emission with LE (NIR region) and HE (visible region). At 78 K, the LE peak reaches 973 nm and the HE peak 752 nm. According to DFT calculations for **2**, the LE emission is tentatively assigned to "{Cu_6S_6} cluster-centered" triplet excited state and the HE emission to "{Cu_6S_6} cluster-to-ligand" charge-transfer triplet excited state. In the literature, solid-state (single) NIR emission is not unusual for transition-metal complexes, including precedents for copper complexes like [Cu_6(mtc)$_6$] (mtc$^-$ = di-*n*-propylmonothiocarbamate) (Sabin et al. 1992), [Cu_6(btt)$_6$] (btt$^-$ = benzothiazolethiolate) (Yue et al. 2009), [Cu_6(Hmna)$_6$] (H_2mna = 2-mercapto-nicotinic acid) (Kundu et al. 2014), and [Cu_4I_4(SbR_3)$_4$] (R = isopropyl and cyclohexyl) (Taylor et al. 2019, 2016). However, report for dual-emission spanning to NIR, like **2**, remains much scarce (Xie et al. 2005).

Conclusions

In this paper, we described the synthesis and successful crystallization of two new Cu(I) complexes supported by monoanionic iminothiolate ligands, *N*-methylbenzimidazolethiolate (Me-bimt$^-$) and formulated [Cu_n(Me-bimt)$_n$], which comprises different metal nuclearity (n = 4 and 6). The crystal structures for both clusters were unambiguously determined by single-crystal X-ray diffraction analysis. Interestingly, the color of the crystals was highly nuclearity-dependent, colorless and deep red for **1** and **2**, respectively, which was rationalized by HOMO–LUMO gaps determined by DFT calculations. Upon UV excitation at room temperature, complexes **1** and **2** gave solid-state photoluminescence with lifetimes of microsecond order. Both complexes displayed temperature-dependent dual emission (78–298 K) in the solid state. The thermochromic dual emission especially found in the entire optical region from visible to NIR is unusual for molecular compounds. The iminothiolate tetra- and hexacopper(I) system reported herein is thus of considerable interest in a new class of optical molecular thermometers

covering a wide range of wavelength. Many other applications may also be anticipated for this class of compounds with a strong advantage for utilizing a naturally-abundant, low-cost transition-metal, copper.

Acknowledgements This work was supported by JSPS KAKENHI Grant no. JP16H06514 (Coordination Asymmetry) and the special research grant from University of Hyogo (2016, 2017). Prof. Morifumi Fujita (University of Hyogo) is acknowledged for useful discussion on ^{1}H NMR spectroscopy.

Compliance with ethical standards

Conflict of interest The authors declare no competing financial interest.

References

Baerends EJ et al (2019) ADF 2019.3, SCM, theoretical chemistry. Vrije Universiteit, Amsterdam

Benito Q et al (2015) Geometry flexibility of copper iodide clusters: variability in luminescence thermochromism. Inorg Chem 54:4483–4494. https://doi.org/10.1021/acs.inorgchem.5b00321

Chivers T, Downard A, Parvez M, Schatte G (2001) Hexameric and tetrameric copper(I) thioamidates. Organometallics 20:727–733. https://doi.org/10.1021/om000809k

De Angelis F, Fantacci S, Sgamellotti A, Cariati E, Ugo R, Ford PC (2006) Electronic transitions involved in the absorption spectrum and dual luminescence of tetranuclear cubane $[Cu_4I_4(pyridine)_4]$ cluster: a density functional theory/time-dependent density functional theory investigation. Inorg Chem 45:10576–10584. https://doi.org/10.1021/ic061147f

Doerge DR, Cooray NM (1991) Synthesis of *N*-substituted benzimidazole-2-thiones. Synth Commun 21:1789–1795. https://doi.org/10.1080/00397919108021578

Farrugia L (2012) WinGX and ORTEP for Windows: an update. J Appl Crystallogr 45:849–854. https://doi.org/10.1107/S0021889812029111

Ford PC, Vogler A (1993) Photochemical and photophysical properties of tetranuclear and hexanuclear clusters of metals with d^{10} and s^2 electronic configurations. ACC Chem Res. https://doi.org/10.1021/ar00028a013

Ford PC, Cariati E, Bourassa J (1999) Photoluminescence properties of multinuclear copper(I) compounds. Chem Rev 99:3625–3647. https://doi.org/10.1021/cr960109i

Huitorel B et al (2018) Evaluation of ligands effect on the photophysical properties of copper iodide clusters. Inorg Chem 57:4328–4339. https://doi.org/10.1021/acs.inorgchem.7b03160

Kitagawa H, Ozawa Y, Toriumi K (2010) Flexibility of cubane-like Cu_4I_4 framework: temperature dependence of molecular structure and luminescence thermochromism of $[Cu_4I_4(PPh_3)_4]$ in two polymorphic crystalline states. Chem Commun 46:6302–6304. https://doi.org/10.1039/c0cc01434f

Kundu T, Jana AK, Natarajan S (2014) Stepwise crystallization: illustrative examples of the use of metalloligands $[Cu_6(mna)_6]^{6-}$ and $[Ag_6(Hmna)_2(mna)_4]^{4-}$ (H_2mna = 2-mercapto nicotinic acid) in the formation of heterometallic two- and three-dimensional assemblies with *brucite*, *pcu*, and *sql* topologies. Cryst Growth Des 14:4531–4544. https://doi.org/10.1021/cg500632d

Nagaoka S, Ozawa Y, Toriumi K, Abe M (2018) A Dual-emission strategy for a wide-range phosphorescent color-tuning of a crystalline-state molecular cluster $[Cu_4I_4(2\text{-Bzpy})_4]$ (2-Bzpy = 2-Benzylpyridine). Chem Lett 47:1101–1104. https://doi.org/10.1246/cl.180435

Perruchas S et al (2010) Mechanochromic and thermochromic luminescence of a copper iodide cluster. J Am Chem Soc 132:10967–10969. https://doi.org/10.1021/ja103431d

Raper ES, Creighton JR, Clegg W (1991) tetrahedro-[Tetrakis {(1-methylimidazoline- 2(3*H*) -thionato) copper(I)}]: electrochemical synthesis, thermal analysis, cyclic voltammetry and crystal structure. Inorg Chim Acta 183:179–187. https://doi.org/10.1016/S0020-1693(00)83012-1

Sabin F, Ryu CK, Ford PC, Vogler A (1992) Photophysical properties of hexanuclear copper(I) and silver(I) clusters. Inorg Chem 31:1941–1945. https://doi.org/10.1021/ic00036a040

Sheldrick G (2015) Crystal structure refinement with SHELXL. Acta Crystallogr Sect C 71:3–8. https://doi.org/10.1107/S2053229614024218

Taylor WV, Soto UH, Lynch VM, Rose MJ (2016) Antimony-supported Cu_4I_4 cuboid with short Cu–Cu bonds: structural premise for near-infrared thermoluminescence. Inorg Chem 55:3206–3208. https://doi.org/10.1021/acs.inorgchem.5b02933

Taylor WV, Cammack CX, Shubert SA, Rose MJ (2019) Thermoluminescent antimony-supported copper-iodo cuboids: approaching NIR emission via high crystallographic symmetry. Inorg Chem 58:16330–16345. https://doi.org/10.1021/acs.inorgchem.9b00229

te Velde G, Bickelhaupt FM, Baerends EJ, Guerra CF, van Gisbergen SJA, Snijders JG, Ziegler T (2001) Chemistry with ADF. J Comput Chem 22:931–967. https://doi.org/10.1002/jcc.1056

Venkatesh V, Pachfule P, Banerjee R, Verma S (2014) Evolution of an adenine-copper cluster to a highly porous cuboidal framework: solution-phase ripening and gas-adsorption properties. Chem Eur J 20:12262–12268. https://doi.org/10.1002/chem.201403115

Xie H, Kinoshita I, Karasawa T, Kimura K, Nishioka T, Akai I, Kanemoto K (2005) Structure study and luminescence thermochromism in hexanuclear 6-methyl-2-pyridinethiolato copper(I) crystals. J Phys Chem B 109:9339–9345. https://doi.org/10.1021/jp0446985

Yam VW-W, Lo KK-W (1999) Luminescent polynuclear d^{10} metal complexes. Chem Soc Rev 28:323–334. https://doi.org/10.1039/a804249g

Yang K, Li S-L, Zhang F-Q, Zhang X-M (2016) Simultaneous luminescent thermochromism, vapochromism, solvatochromism, and mechanochromism in a C_3-symmetric cubane $[Cu_4I_4P_4]$ cluster without Cu–Cu interaction. Inorg Chem 55:7323–7325. https://doi.org/10.1021/acs.inorgchem.6b00922

Yue C, Yan C, Feng R, Wu M, Chen L, Jiang F, Hong M (2009) A polynuclear d^{10}–d^{10} metal complex with unusual near-infrared luminescence and high thermal stability. Inorg Chem 48:2873–2879. https://doi.org/10.1021/ic801840g